

## SATELLITE ACCELEROMETER MEASUREMENTS OF NEUTRAL DENSITY AND WINDS DURING GEOMAGNETIC STORMS

Frank A. Marcos  
Air Force Geophysics Laboratory  
Hanscom Air Force Base  
Bedford, MA 01731

and  
Jeffrey M. Forbes  
Department of Electrical, Computer, and Systems Engineering  
Boston University  
Boston, MA 02215

A new thermospheric wind measurement technique is reported which is based on a Satellite Electrostatic Triaxial Accelerometer (SETA) system capable of accurately measuring accelerations in the satellite's in-track, cross-track and radial directions. Data obtained during two time periods are presented. The first data set describes cross-track winds measured between 170 and 210 km during a 5-day period (25-29 March 1979) of mostly high geomagnetic activity. In the second data set, cross-track winds and neutral densities from SETA and exospheric temperatures from the Millstone Hill incoherent scatter radar are examined during an isolated magnetic substorm occurring on 21 March 1979.

A polar thermospheric wind circulation consisting of a two-cell horizontal convection pattern is reflected in both sets of cross-track acceleration measurements. Winds are generally trans-polar and parallel to the 1600h/0400 MLT meridian with return flows in the morning and evening sectors near  $57^\circ$  and  $70^\circ$  geomagnetic latitude, respectively. Winds are of order  $100\text{-}200\text{ ms}^{-1}$  during quiet periods, and attain maximum speeds of order  $300\text{-}600\text{ ms}^{-1}$  during storm conditions. The two-cell pattern is distinctively more well-ordered in geomagnetic rather than geographic coordinates. The substorm circulation pattern persists almost unattenuated for about 6 hours after the magnetic disturbance has returned to quiet levels.

The density response is highly asymmetric with respect to its day/night behavior. At high geomagnetic latitudes ( $>60^\circ$ ) the daytime density variation, about a 40% increase from quiet levels, distinctively reflects the response to an increase in magnetic activity with a time delay of less than 3 hours. At lower latitudes the response is smaller (20%) and less well-defined, occurring with a time delay of about  $6 \pm 2$  hours near  $10\text{-}20^\circ$  latitude. The nighttime density response, on the other hand, is not so well defined poleward as it is equatorward of  $60^\circ$  latitude. The time delay increases from about  $2 \pm 2$  hours to  $6 \pm 2$  hours from high to low latitudes. An exospheric temperature response occurs at Millstone Hill ( $42^\circ\text{N}$ ) with an amplitude of  $210^\circ\text{K}$  and time delay of between 0 and 2.5 hours.

Latitude structures of the density response at successive times following the substorm peak suggest the equatorward propagation of a disturbance with a phase speed of between  $300$  and  $600\text{ ms}^{-1}$ . A deep depression in the density at high latitudes ( $>70^\circ$ ) is evident in conjunction with this phenomenon. The more efficient propagation of the disturbance to lower latitudes during the night is probably due to the "midnight surge" effect.

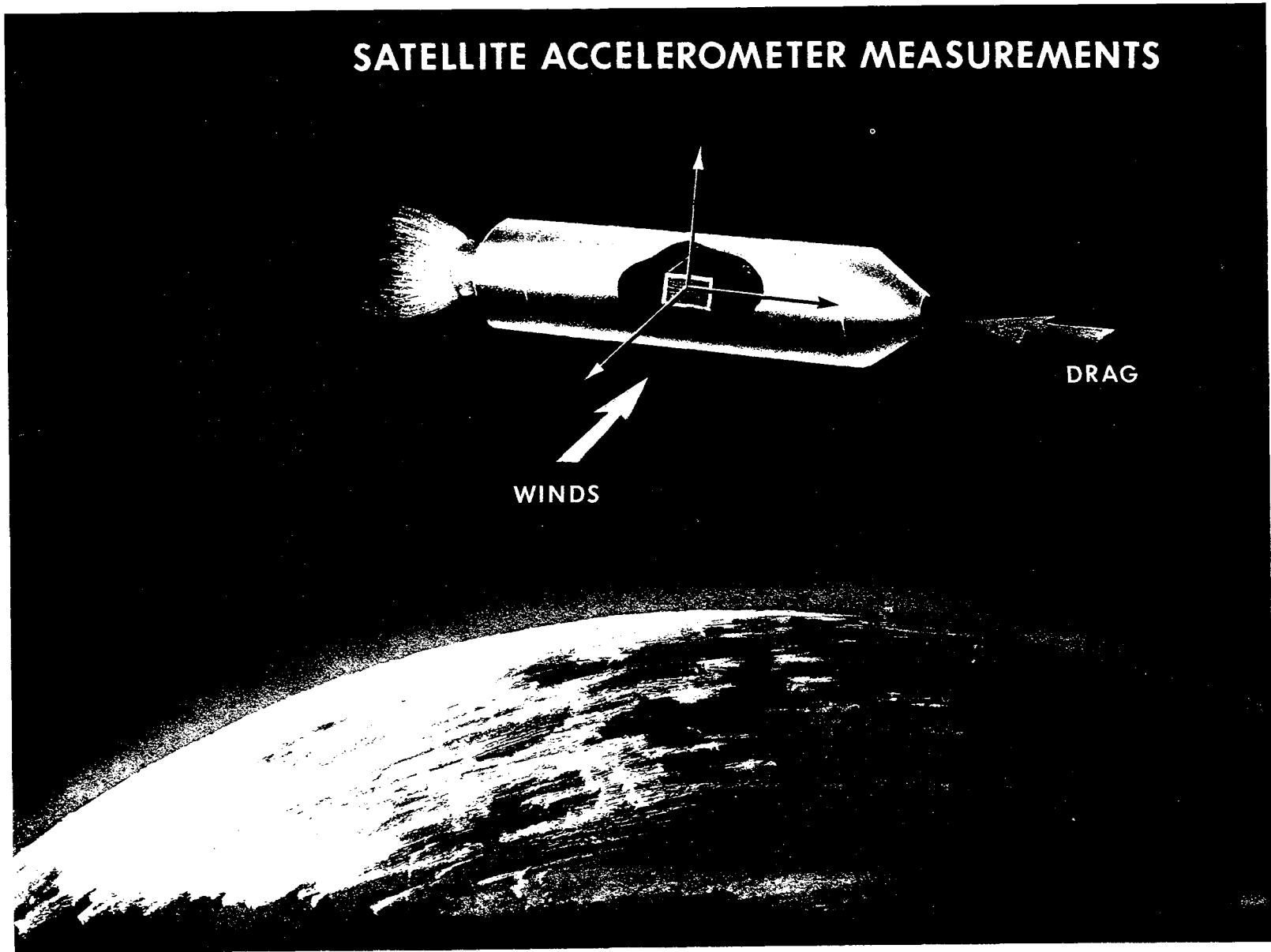


Figure 1. Cartoon showing orientation of accelerometer axes with respect to aerodynamic drag and cross-track wind vectors.

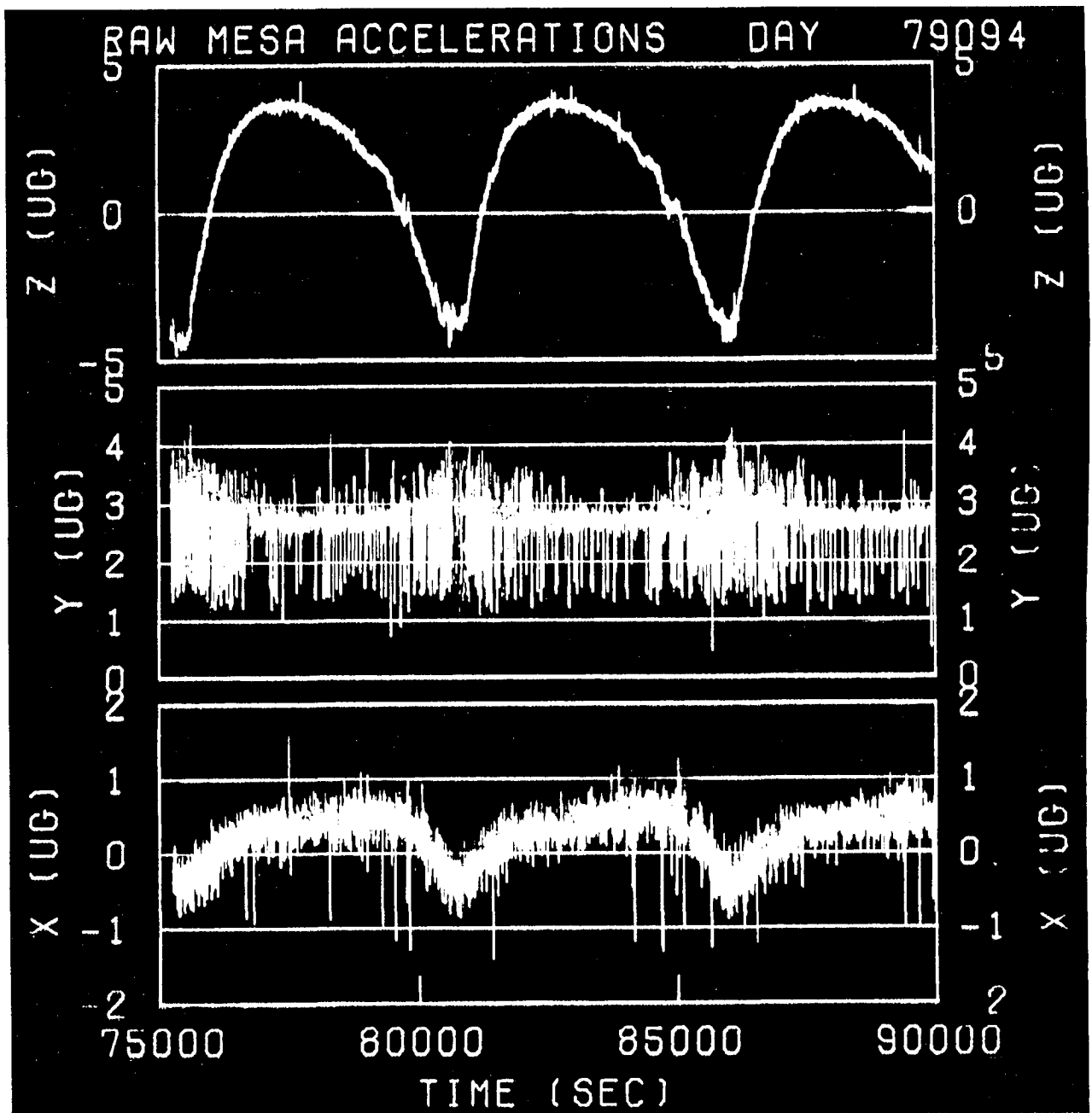


Figure 2. Raw acceleration data from each accelerometer axis plotted as a function of time. Period covered is almost three full orbits. The top frame shows accelerations measured in the along-track (Z) direction. Larger accelerations are indicated by larger negative values. Thus satellite minimum altitudes (and maximum drags) occur near 80500 and 85900 seconds.

## First Data Set: period of mostly high geomagnetic activity

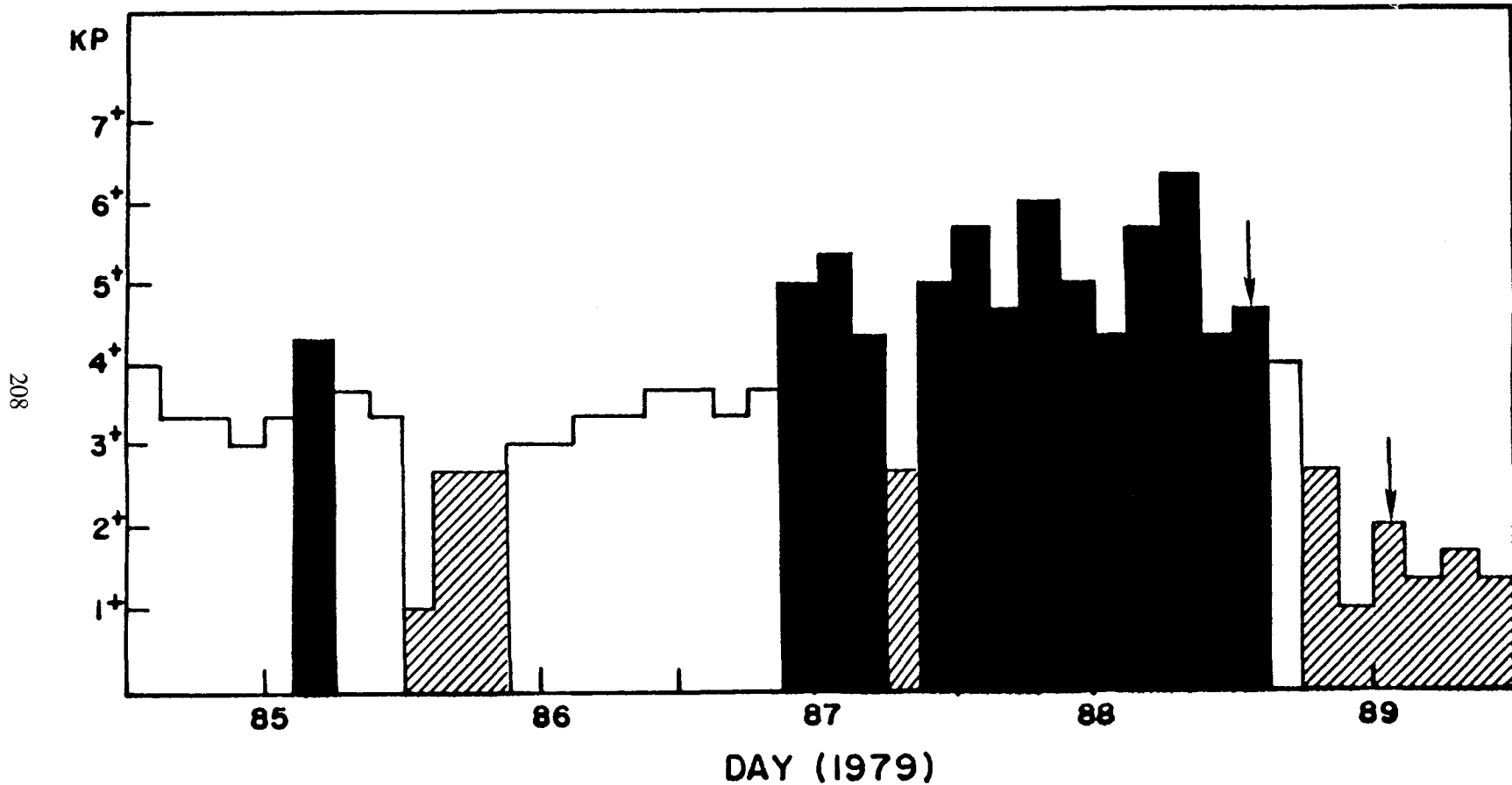


Figure 3. Kp variation during a 5-day period during 1979. Cross-hatched and solid areas represent Quiet ( $K_p \leq 3$ ) and Active ( $K_p \geq 5$ ) periods, respectively. Vertical arrows denote periods of the first data set analyzed.

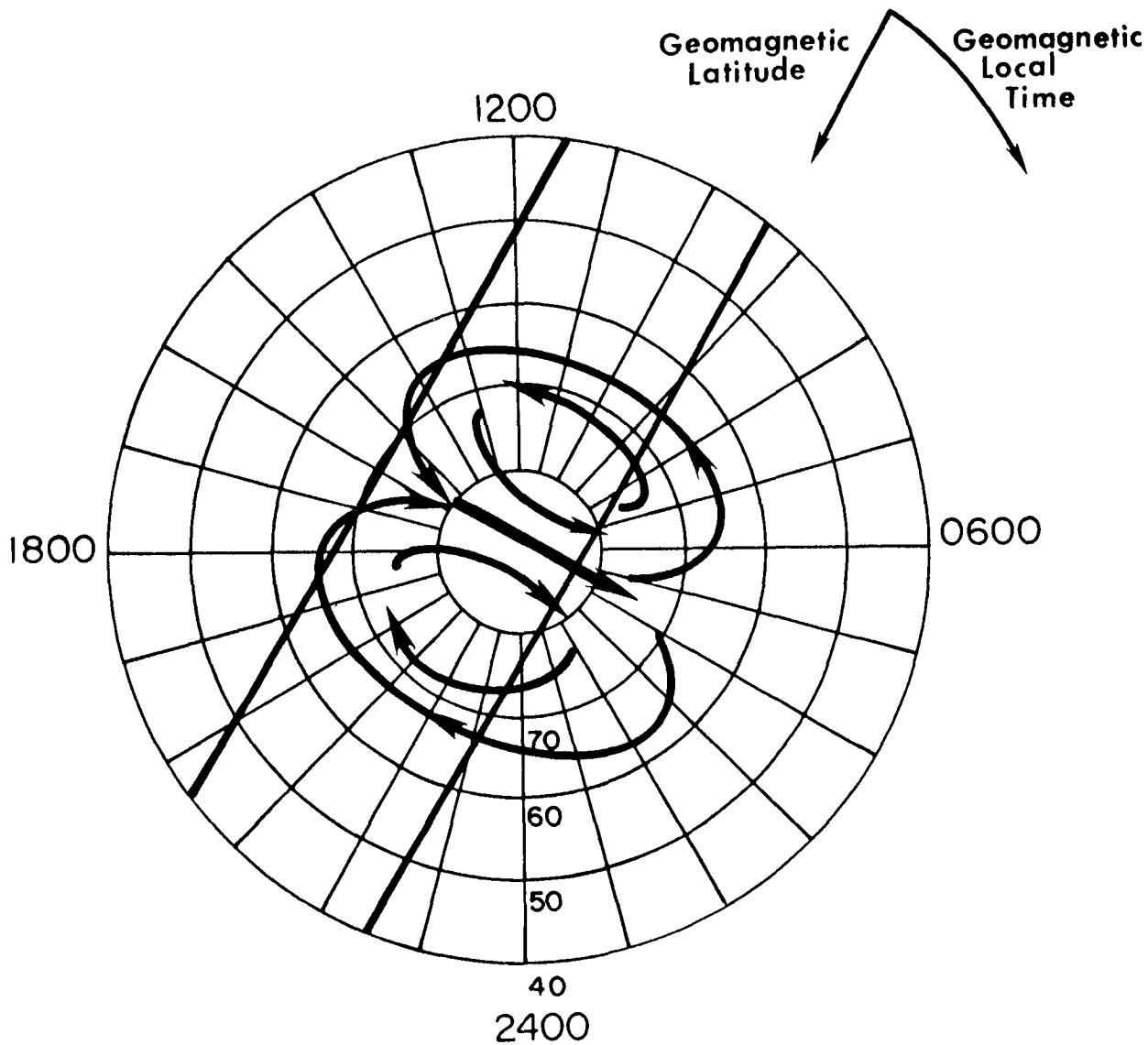
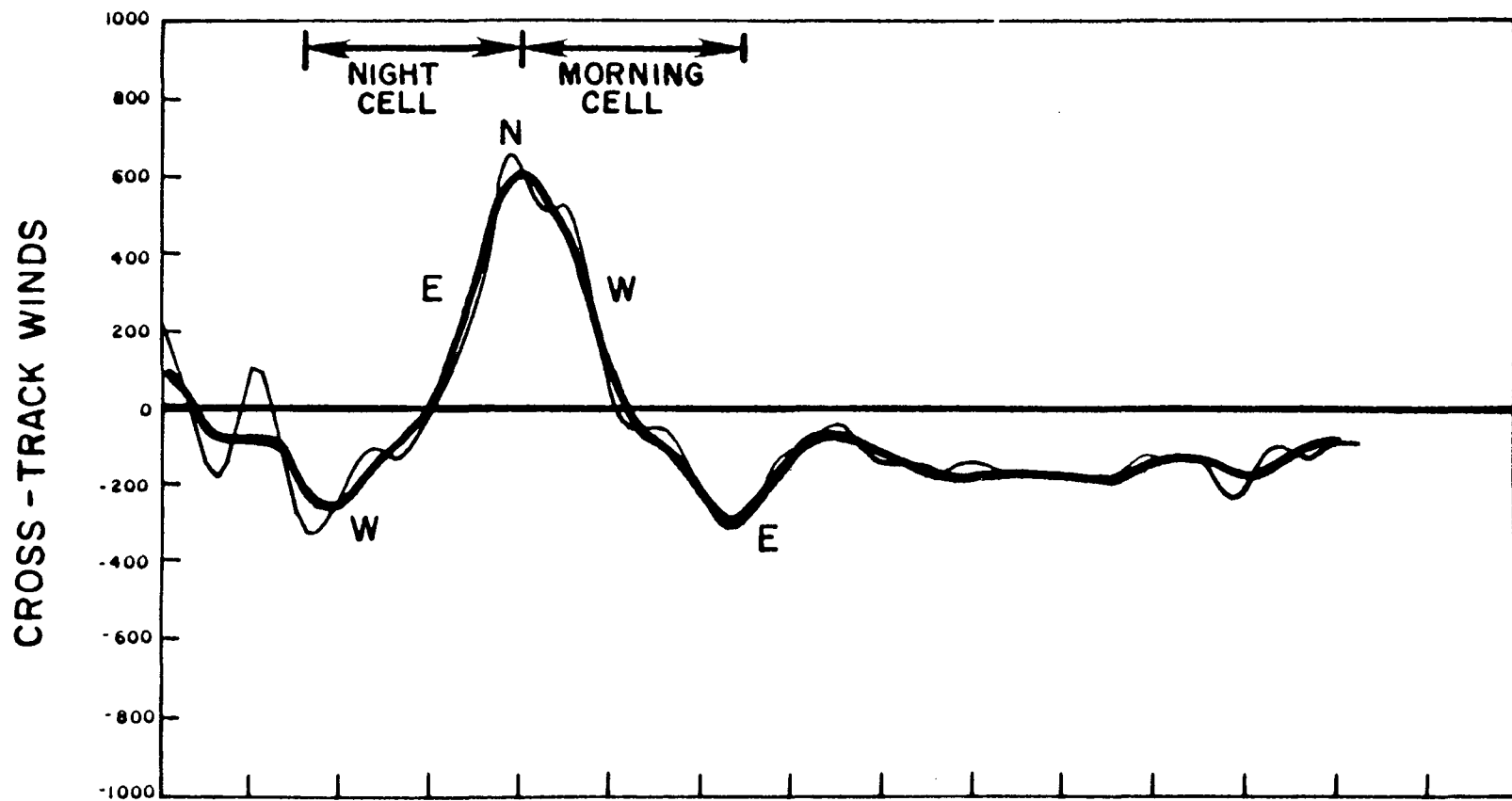


Figure 4. Schematic of 2-cell polar lower thermospheric circulation pattern in geomagnetic latitude and local time coordinates. Parallel lines represent bands of satellite tracks during 5-day period under study.

# DAY 79088



GMTMM	2400	2403	2407	2410	2413	2417	2420	2423	2427	2430	2433	2437	2440	2443	2447	2450
GGLAT	30	44	57	70	82	80	67	55	41	27	13	-1	-14	-27	-41	-55
GMLAT	39	53	67	79	87	73	59	46	32	18	4	-11	-23	-37	-51	-65
LT	2159	2150	2134	2105	1860	1244	1115	1060	1036	1027	1020	1014	1008	1001	952	938
ALT	220.2	213.5	206.6	200.0	192.5	185.7	179.4	174.4	170.7	169.8	172.6	179.5	189.0	202.3	217.1	232.2

SETA-1 CROSS-TRACK WIND DATA

Figure 5. Cross-axis winds, corresponding to geomagnetically disturbed conditions, plotted vs. GMT, geographic latitude (GGLAT), geomagnetic latitude (GMLAT), local time (LT), and altitude (ALT). Unsmoothed (light line) and smoothed (heavy line) data are shown. E, W, N refer, respectively to the fact that cross-track accelerations are due primarily to Eastward, Westward, and Northward flows.

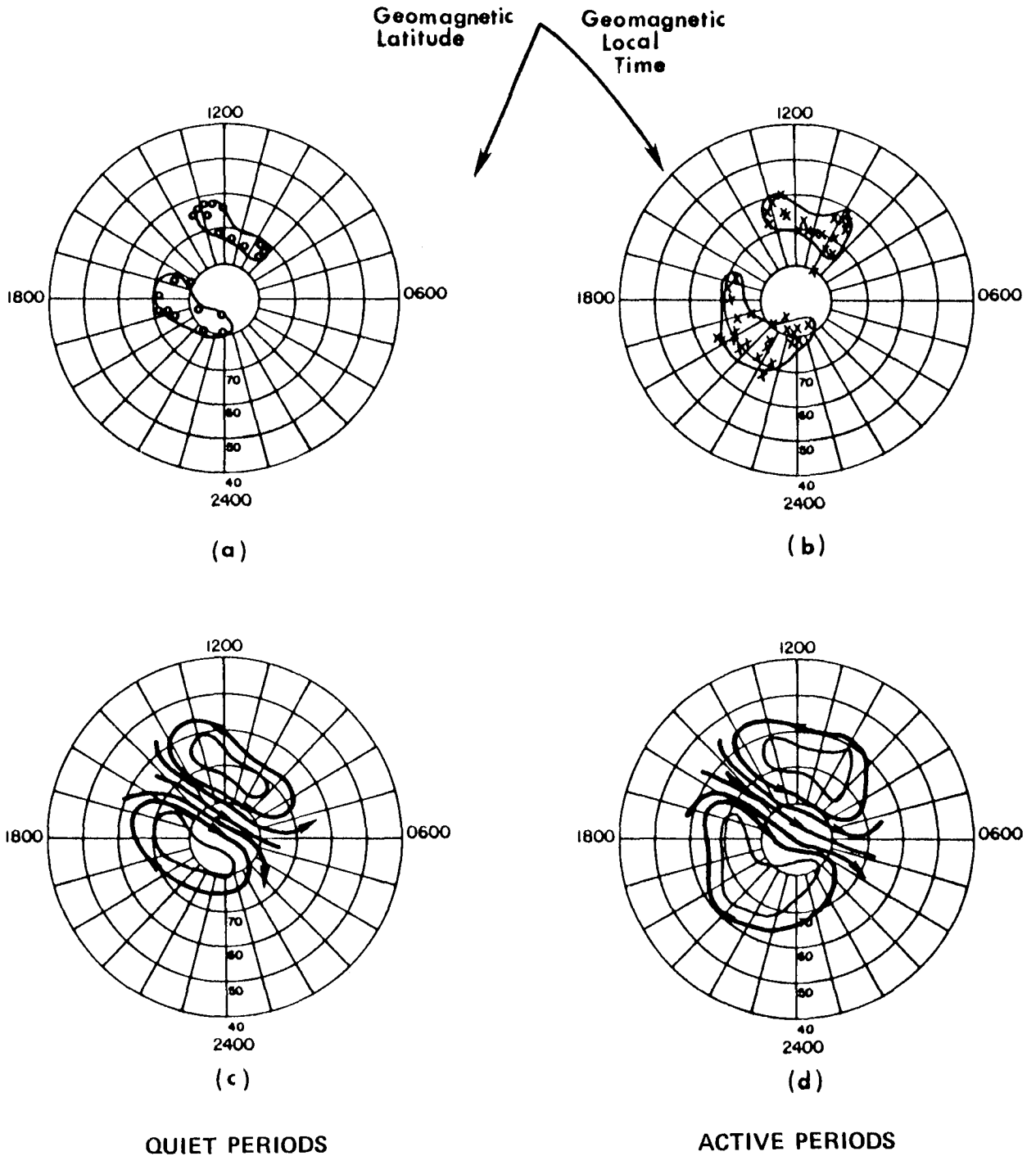


Figure 6. (a) and (b): “cell centers” of double-vortex circulation system for quiet and active geomagnetic conditions, respectively. (c) and (d): schematics of 2-cell circulation patterns consistent with the quiet and active period data, respectively.

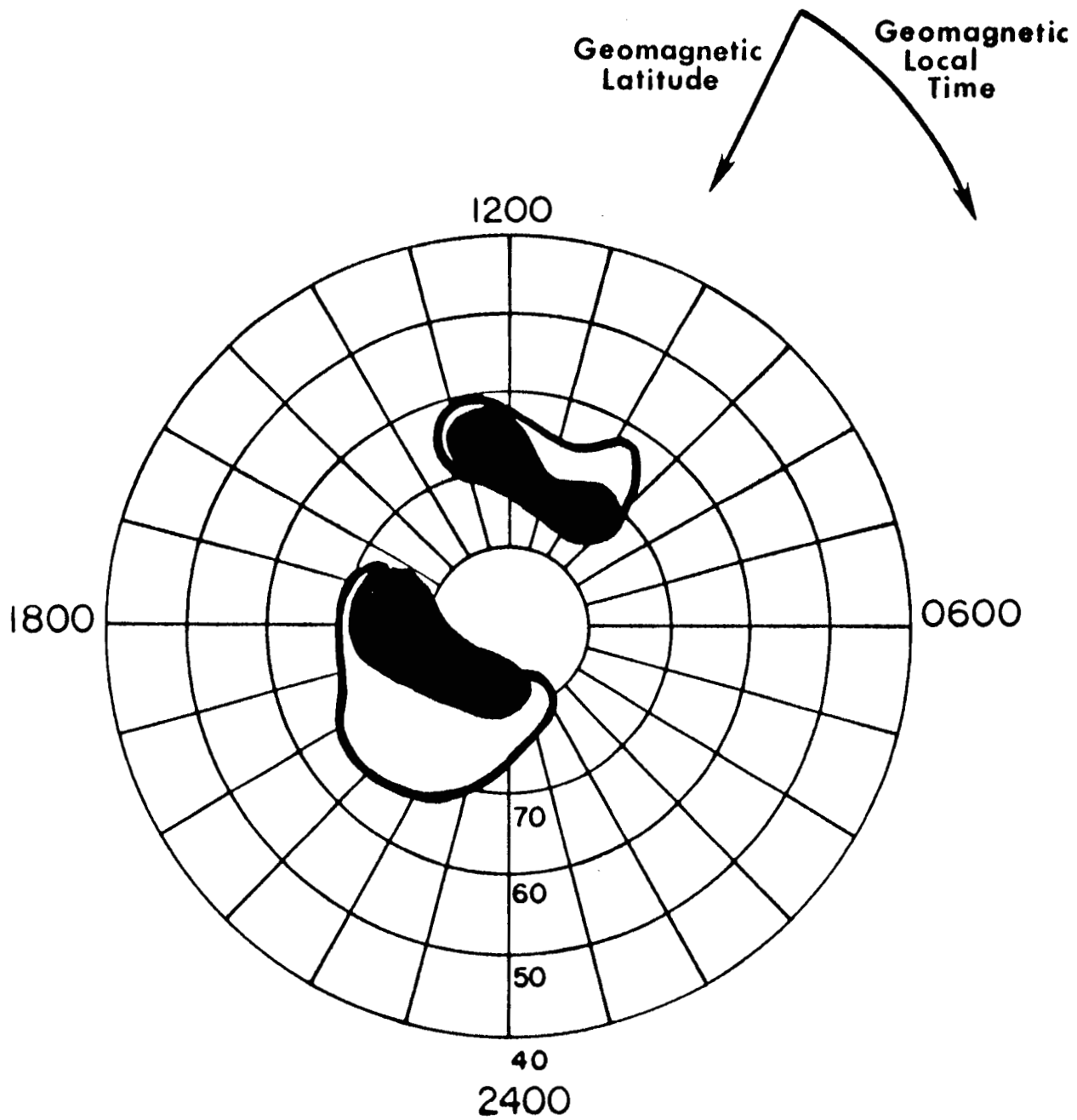
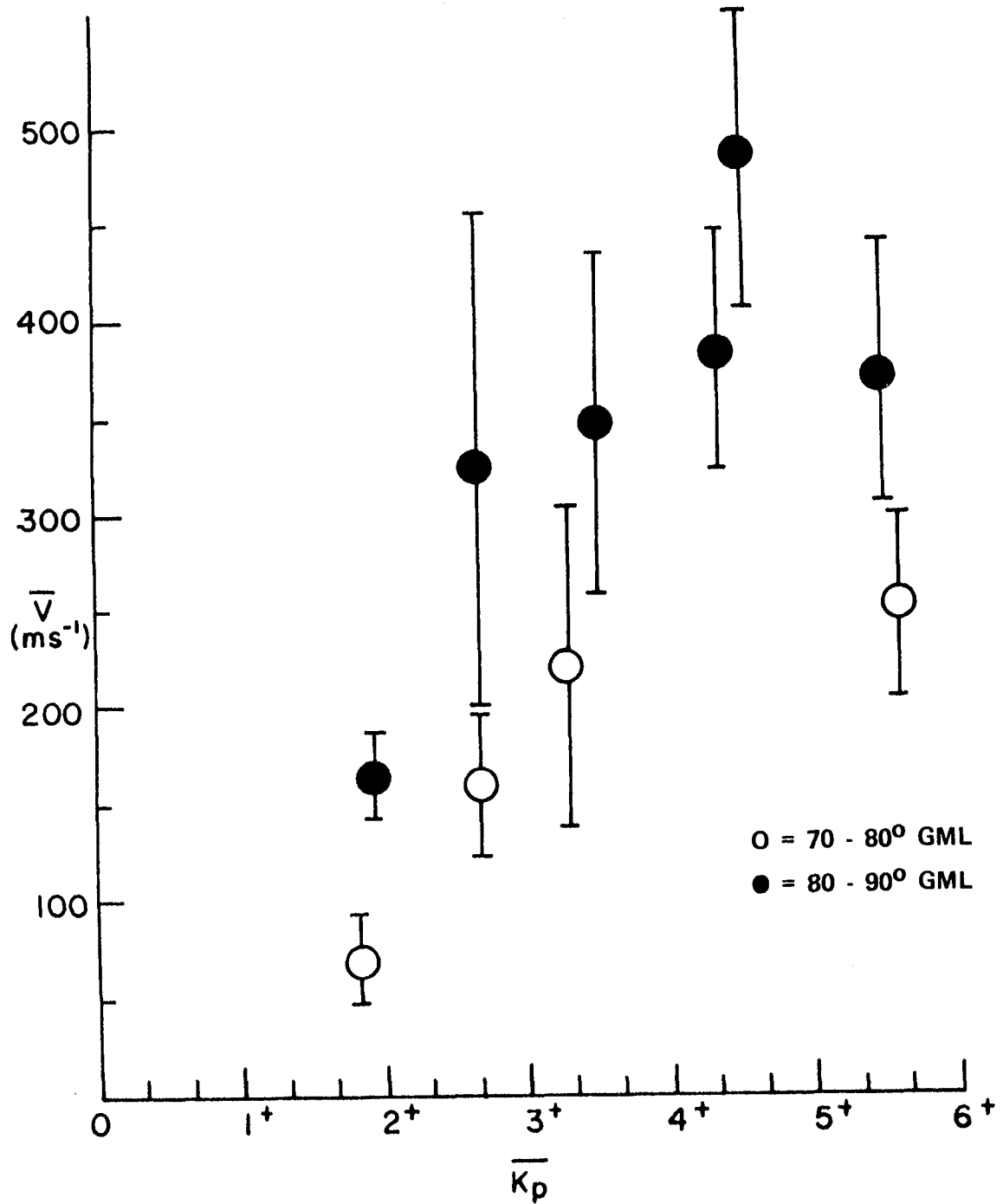


Figure 7. A comparison between areas including "cell centers" for quiet (black) and active (white) conditions.





**AVERAGE WIND VELOCITY VS.  $K_p$**

Figure 8. Average wind data plotted vs. the corresponding average  $K_p$  values. Solid and open circles represent, respectively, measurements taken between 80-90° and 70-80° GMLAT. Standard deviations of the means are also indicated.

## SUMMARY OF WINDS RESULTS FROM FIRST DATA SET

1. SATELLITE ACCELEROMETER CROSS-TRACK WIND DATA ARE USED TO INFER LOWER THERMOSPHERE CIRCULATION PATTERNS
2. MAIN FLOW IS ORIENTED PARALLEL TO 1600/0400 GLT MERIDIAN
3. TWO-CELL SYSTEM COVERS GREATER AREA OF POLAR CAP DURING ACTIVE CONDITIONS
4. WIND INTENSITY TENDS TO INCREASE WITH GEOMAGNETIC ACTIVITY

Figure 9. Summary of wind results from first data set.

## Second Data Set: isolated substorm

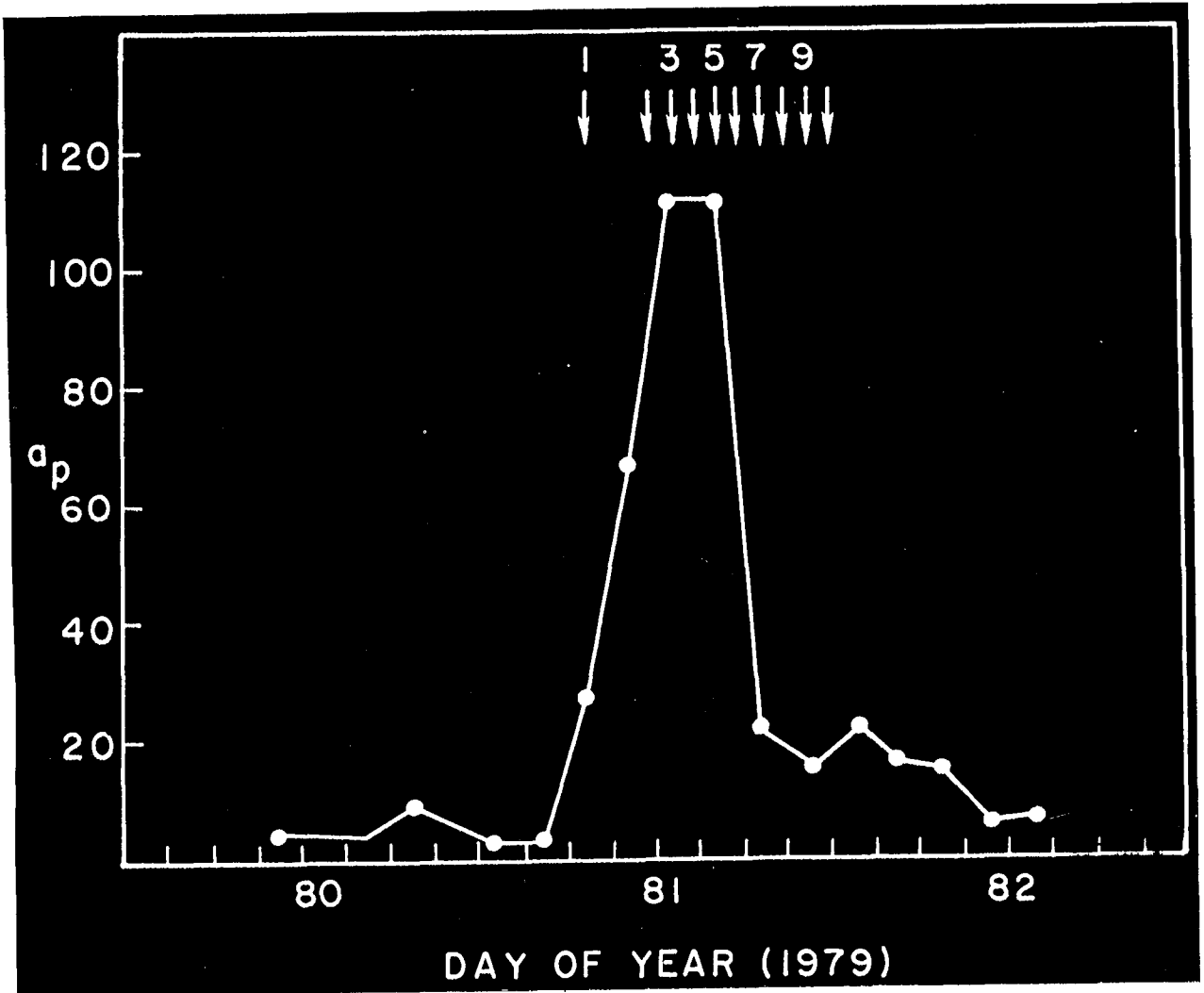


Figure 10. Variation of the 3-hourly planetary magnetic index  $a_p$  during the substorm under study. Vertical arrows indicate orbits (actually, times of polar crossings) which are explicitly included in the analysis of this paper.

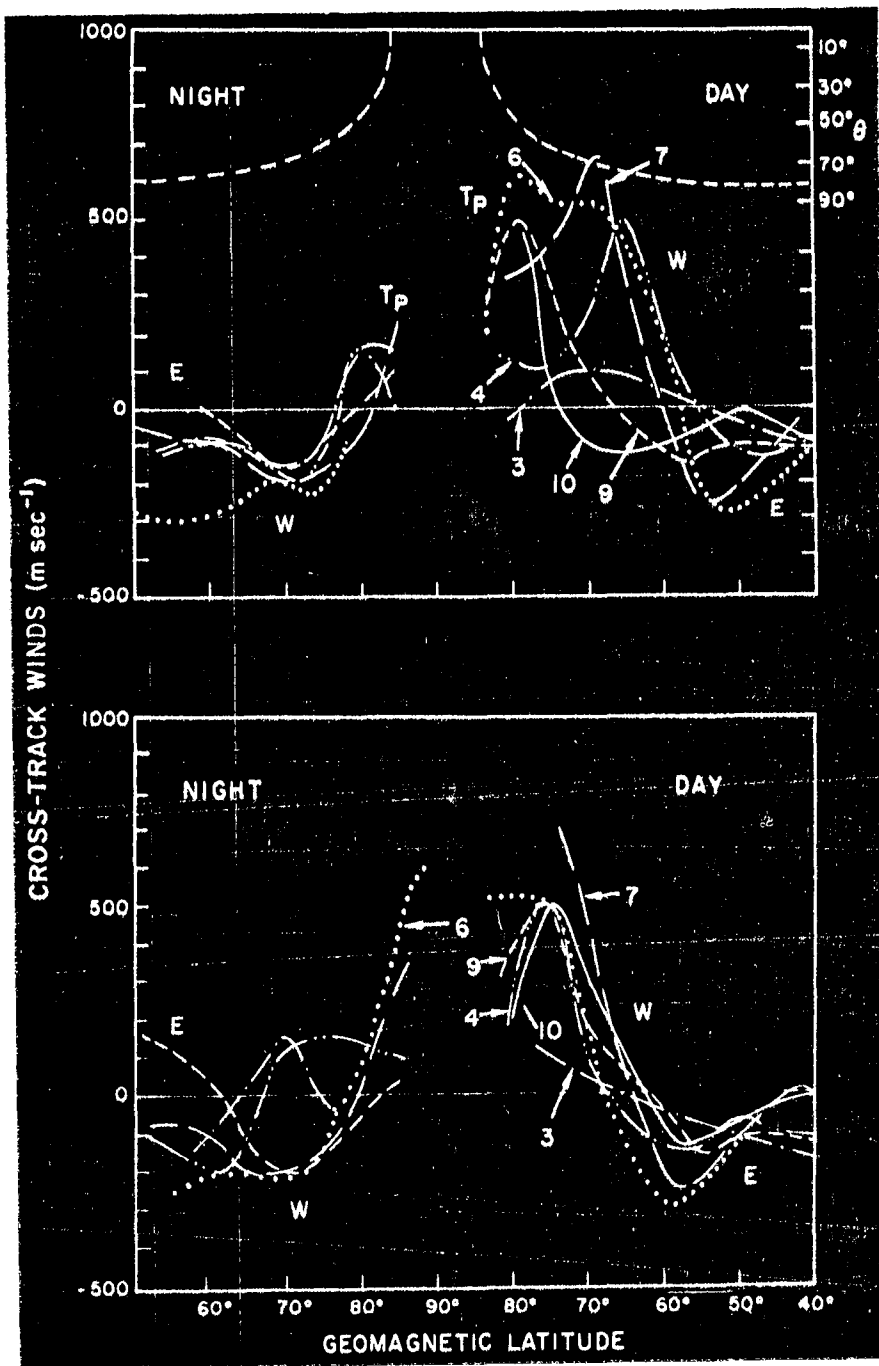


Figure 11. Cross-track winds from selected orbits (3, 4, 6, 7, 9, 10) as a function of geographic (top) and geomagnetic (bottom) latitudes. "E" denotes east-ward oriented winds, "W" denotes westward-oriented winds, and TP indicates trans-polar oriented winds. The angle  $\theta$  plotted as a dashed line in the top figure represents the relative orientation of the cross-track direction and the geographic meridian.

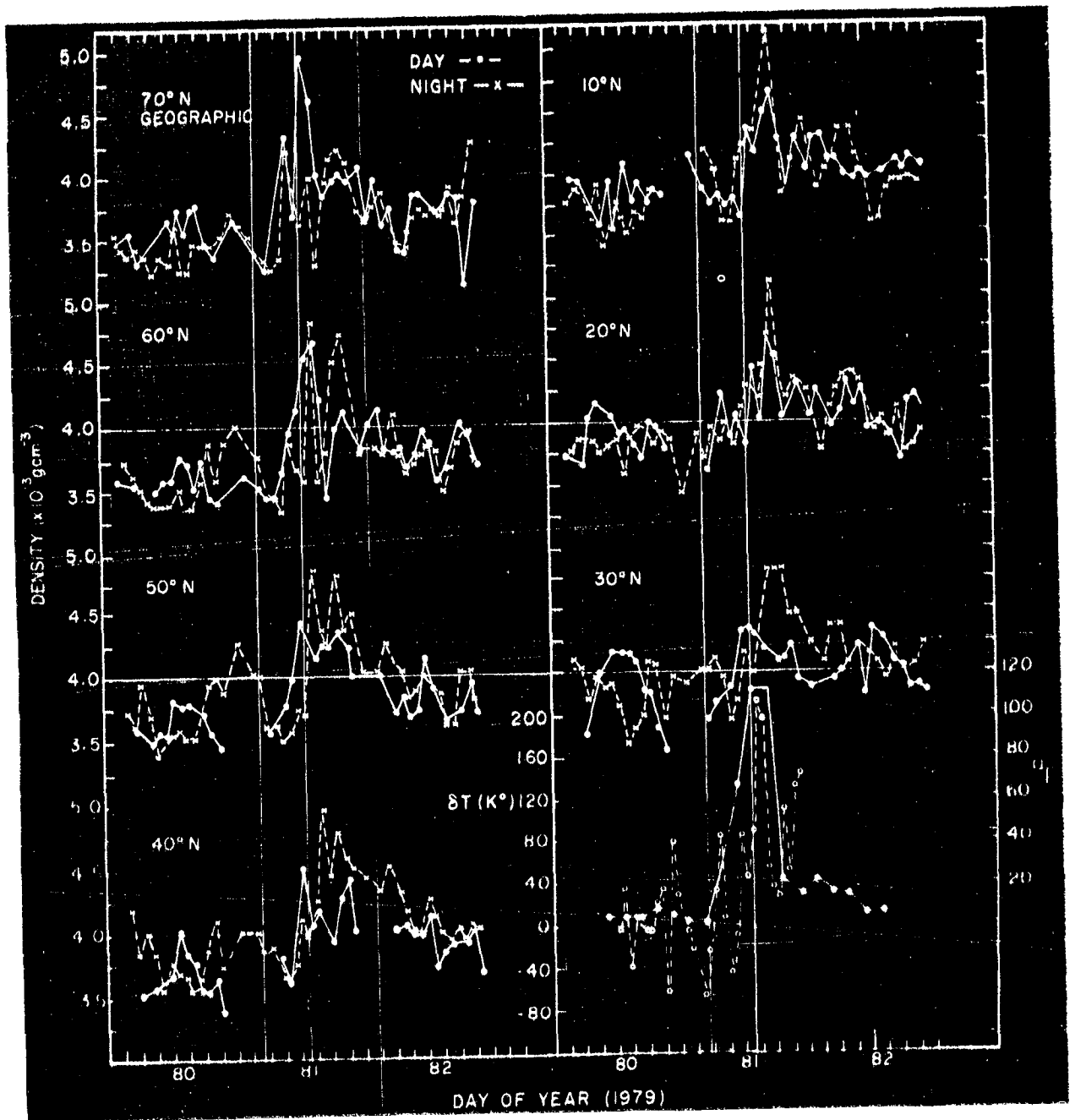


Figure 12. Temporal response of density at various geographic latitudes for day and night crossings. Exospheric temperatures from Millstone Hill and the  $a_p$  index are plotted in the bottom right hand frame of the figure. For reference, vertical lines are drawn through the "last quiet" and "first maximum" values of  $a_p$ .

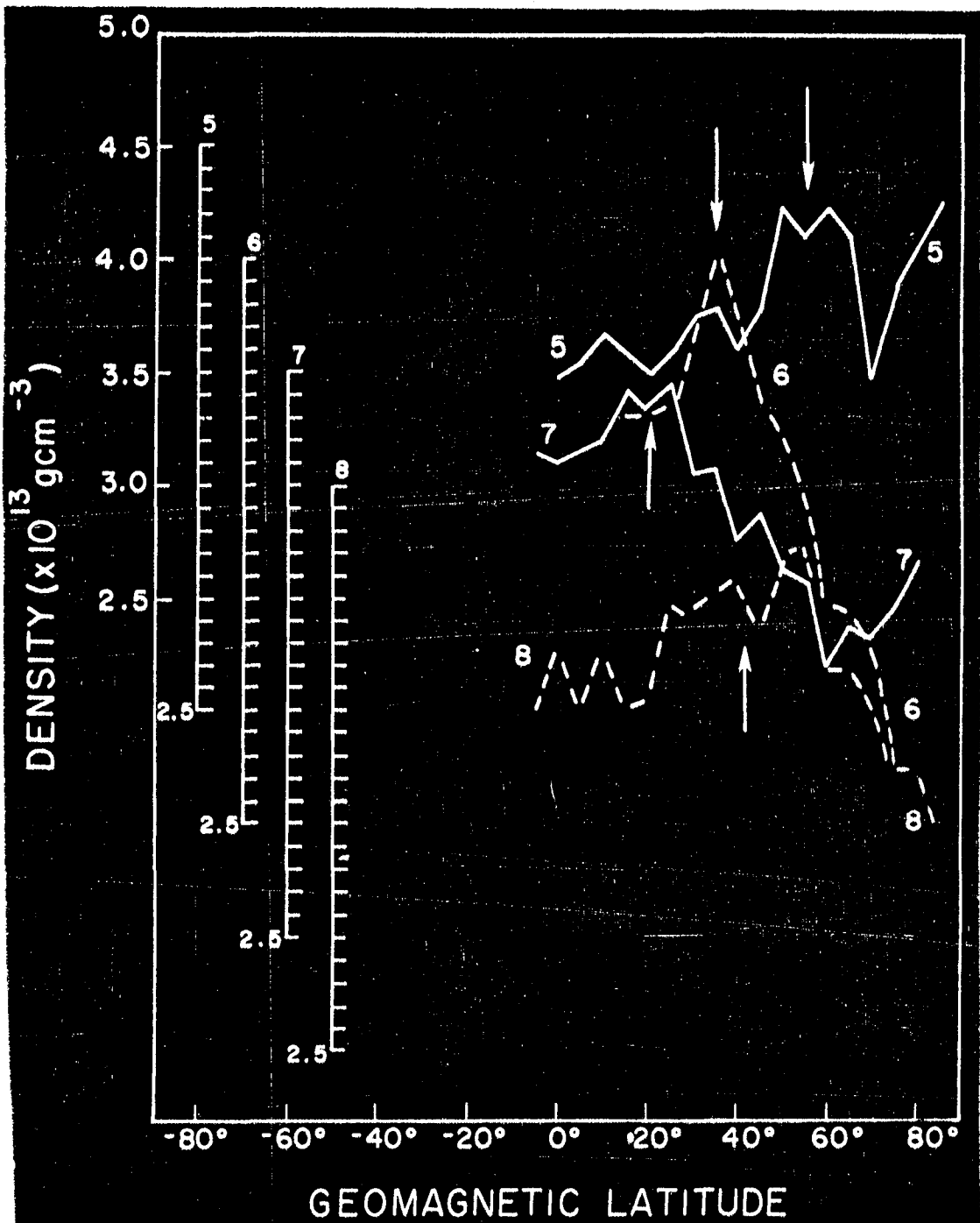


Figure 13. Nighttime density responses for orbits 5, 6, 7, 8 as a function of geomagnetic latitude. Vertical arrows indicate approximate latitudes corresponding to density bulge associated with propagating disturbance launched during the substorm.

## CONCLUSIONS

1. SATELLITE ACCELEROMETER PROVIDES SIMULTANEOUS  
NEUTRAL DENSITY AND CROSS-TRACK WINDS
2. TRANS-POLAR WINDS IN LOWER THERMOSPHERE ARE  
PARALLEL TO 1600/0400 GLT MERIDIAN
3. WIND PATTERNS CAN PERSIST FOR SEVERAL HOURS  
AFTER STORM PERIOD
4. NEUTRAL DENSITY DATA SHOW EVIDENCE OF  
"MIDNIGHT SURGE" EFFECT
5. GRAVITY WAVE SIGNATURES ARE OBSERVED AT  
HIGH AND MIDDLE LATITUDES

Figure 14. Conclusions from analysis of both data sets described in this paper.